Four-Wave-Mixing in Zirconia-Yttria-Aluminum Erbium Codoped Silica Fiber

H. Ahmad harith@um.edu.my — Photonics Research Centre, Physics Department, University of Malaya, 50603 Kuala Lumpur, Malaysia

M. C. Paul — Fiber Optics and Photonics Division, Central Glass & Ceramic Research Institute-CSIR, Kolkata, India

N. A. Awang — Faculty of Science, Technology and Human Development, Universiti Tun Hussein Onn Malaysia, 86400 Batu Pahat, Johor

S. W. Harun — Department of Electrical Engineering, Faculty of Engineering, University of Malaya, 50603 Kuala Lumpur Malaysia

M. Pal — Fiber Optics and Photonics Division, Central Glass & Ceramic Research Institute-CSIR, Kolkata, India

K. Thambiratnam — Photonics Research Centre, Physics Department, University of Malaya, 50603 Kuala Lumpur, Malaysia

The generation and characterization of the Four-Wave-Mixing (FWM) effect in an Erbium Doped Zirconia-Yttria-Alumino Silicate Fiber (EDZF) is described. The EZDF is fabricated from a conventional silica preform by Modified Chemical Vapour Deposition (MCVD) and also solution doping to add glass modifiers and nucleating agents, with the resulting preform annealed and drawn into a fiber strand with a 125 ± 0.5 μm diameter. A 4 m long EZDF, ZEr-B with a propagation loss of 0.68 dB/m and an erbium concentration of 3000 ppm is used to investigate the FWM effect. The FWM power levels are measured to be approximately - 45 dBm at a region of 1565 nm and show good agreement with the theoretical predicted values. A non-linear coefficient of 14 $W^{-1}km^{-1}$ is also measured, along with chromatic and slope dispersion values of 28.45 ps/nm.km and 3.63 ps/nm^2.km, which agree with the predicted values. The fabricated ZEr-B fibre has many potential applications utilizing the FWM effect, including the generation of multi-wavelength outputs.
[DOI: http://dx.doi.org/10.2971/jeos.2012.12011]

Keywords: Zirconia-Erbium doped fiber, non-linear optical phenomena, four-wave-mixing

1 INTRODUCTION

Fiber Optical Amplifiers (FOAs) are a key component in realizing the deployment of long range, high-speed and large capacity communication networks [1, 2]. FOAs are able to effectively counter the attenuation and distortion of multiple signals travelling in optical transmission fibers at the same time [2] and have been widely used in Dense Wavelength Division Multiplexing (DWDM) and Optical Time Division Multiplexing (OTDM) systems. Furthermore, recent advances in technology have also opened up new possibilities for FOAs in a multitude of applications, including the generation of single and multi-wavelength outputs [3, 4], wavelength conversion [5] and wide-band spectral sources [6].

The development of in-line optical amplification was necessitated by the need to overcome the switching and processing limitations of electronic regenerators which were the dominant means of amplification at the time [7, 8]. Initially, research efforts focused on methods such as Raman amplification [9, 10] Semiconductor Optical Amplifiers (SOAs) [11, 12] and Fiber Optic Parametrical Amplifiers (FOPAs) [13, 14] to amplify optical signals, but the cost and complexity of these methods made them commercially impractical. It was not until the early 1990s that a low-cost and commercially viable alternative was developed in the form of the Erbium Doped Fiber Amplifier (EDFA) [1]. EDFAs are capable of providing a wide amplification bandwidth and can be easily spliced to conventional silica fibers, making them the backbone of many optical networks worldwide.

Current research efforts have now focused towards the development of compact, high performance and low cost EDFAs. In this regard, new fibres such as thulium, phosphorus, tellurite, bismuth and photonic crystal fibres [15]-[20] have been explored to increase the erbium ion concentration in the fiber without detrimental effects such as concentration quenching [21] and cluster formation [22]. However, these new fibres are not without their drawbacks, for instance thulium and bismuth based fibers that cannot be spliced easily to conventional SMFs. In this regard, Zirconia has been seen as a highly promising candidate in the development of compact, high erbium concentration EDFAs. Zirconia or ZrO_2 ions co-doped in silica fibers possess a high index of refraction that has been reported of around 1.45 over the visible and near infrared spectrum [23, 24]. As such, ZrO_2 ions tend to exhibit wide emission and absorption bandwidths, as predicted by the Fuchtbauer-Ladenberg relationship [25, 26] and JuddOfelt theory [27, 28]

Received January 10, 2012; revised ms. received February 18, 2012; published May 08, 2012 ISSN 1990-2573

and therefore can amplify more DWDM channels than lower index materials. Furthermore, zirconia has excellent mechanical strength and is chemical corrosion resistance as well as being non-hygroscopic, is easily spliced to SMFs and exhibits excellent transmission in the visible and near infrared; giving the zirconia doped EDFA practical applications in the real world. The fabrication and characterization of an Erbium Doped Zirconia-Yttria-Alumino Silicate Fiber (EDZF) is the focus of the first part of this work.

Additionally, zirconia co-doped fibers have also been shown to exhibit significant non-linear characteristics. These non-linear characteristics, which are not seen in conventional Single-Mode Fibres (SMFs) or EDFAs, [1] have tremendous potential for the development of various new applications such as multi-wavelength outputs and also wavelength conversion. Of particular interest is the Four-Wave Mixing (FWM) effect. In the absence of significant photo-absorption effects, FWM is a type of optical Kerr effect, and occurs when light at two or more different wavelengths is launched into a fiber [1]. The FWM effect is observed when signals at different wavelengths are launched into a fiber, and the interaction of these two signals gives rise to a new signal (known as an idler), the wavelength of which does not coincide with any of the others [29, 30]. The FWM effect has tremendous potential for the development of new fiber based wavelength sources, and is the focus of the later part of this work.

2 ZIRCONIA YTTRIA-ALUMINO SILICATE GLASS FABRICATION

The EDZF is fabricated in three stages. In the first stage, a conventional silica preform is fabricated using the Modified Chemical Vapour Deposition (MCVD) technique, whereby $SiCl_4$ and P_2O_5 vapors are passed through a slowly rotating silica tube that is heated by an external burner. The burner heats the length of the tube as it rotates and, due to the high temperature generated, the chloride in the $SiCl_4$ and P_2O_5 vapors oxidizes, depositing a porous phospho-silica layer along the inner wall of the silica tube. The optimum deposition temperature range for the MCVD process is 1350 - 1400 °C, with a variation of the pre-sintering temperature from 1300 to 1450 °C. The fabricated silica tube, with its deposited porous phospho-silica layer, then undergoes a solution doping process using dopant precursors of suitable strength to obtain the optimized process parameters for making a fiber with a Numerical Aperture (NA) of approximately 0.17 - 0.20. The glass modifiers, ZrO_2, Y_2O_3, Al_2O_3 and Er_2O_3 are individually mixed with alcohol and water at a ratio of 1:5 to form the complex ions $ZrOCl_2.8H_2O$, $YCl_3.6H_2O$ $AlCl_3.6H_2O$ and $ErCl_3.6H_2O$ respectively and are then incorporated into the host matrix using the solution doping technique. Small quantities of Y_2O_3 and P_2O_5 are also added to the glass matrix to act as nucleating agents, functioning to increase the phase separation of the Er_2O_3 doped micro-crystallites that will form in the core matrix of the optical fiber preform.

During the fabrication process, it is crucial to note that, in a bulk glass matrix, pure zirconia exists in three distinct crystalline phases over different temperature ranges. At very high temperatures, above 2350 °C, ZrO_2 has a cubic structure whereas, at intermediate temperatures between 1170 and 2350 °C, a tetragonal structure is observed. At low temperatures, below approximately 1170 °C, ZrO_2 takes on a monoclinic structure. The transformation of the crystalline structure from tetragonal to monoclinic is very rapid and is accompanied by a 3 to 5 percent volume increase. This rapid increase can result in extensive cracking in the material - as was observed in the doped core region of the preform after the fabrication - and is highly detrimental, as it destroys the mechanical properties of fabricated components during cooling. In order to overcome this problem, several oxides, such as MgO, CaO, and Y_2O_3 that dissolve in the zirconia crystal structure can be used to slow down or eliminate these crystal structure changes; in this work a minor quantity of Y_2O_3 is used.

In the final stage of the fiber fabrication process, the fabricated preform that has undergone the solution doping process is annealed at 1100 °C for 3 hours in a closed furnace, under heating and cooling rates of 20 °C/min, to generate ErO_2 doped ZrO_2 rich micro-crystalline particles. The resulting annealed preform is collapsed into a solid rod at a temperature higher than 2000 °C and is drawn into a fiber strand with a diameter 125 ± 0.5 μm, using a conventional fiber drawing tower. During the drawing process, the preform (and the fiber obtained) is exposed to a temperature of around 2000 °C for only a few minutes. Due to the high cooling rate of the material and the melting temperature of the ZrO_2 crystals being above 2200 °C, the ZrO_2 nano-crystalline host is retained within the silica glass matrix. Both the primary & secondary coatings were applied on-line to increase the tensile strength, as well as to reduce the moisture ingress from external sources. During the fiber drawing procedure, proper control of the fiber diameter, coating thickness and coating concentricity along the whole length of the fabricated fiber gives the optimization required for the production of a high quality optical fiber. The thickness of the primary coating (Desolite DP-1004), as well as that of the secondary coating (Desolite DS-2015), and the coating uniformity were ensured by adjusting the flow pressure of the inlet gases into the primary and secondary coating resin vessels during the drawing of the fiber, as well as by properly aligning the position of primary and secondary coating cup units.

3 EZDF CHARACTERISATION

In bulk zirconia-silicate glass, phase-separation has been observed at temperatures below the onset of crystallization - which also results in structural inhomogeneity [31, 32]. Phase separation, or immiscibility, is a phenomenon that is known to exist in amorphous binary systems [33]; however in some ZrO_2-SiO_2 systems immiscibility exists even in the stable liquid phase above the melting point. The phase diagram of ZrO_2-SiO_2 systems was evaluated using Fact-Sage software, and it was determined that a stable immiscibility zone exists in the range between 60 and 80 mole % SiO_2. This stable immiscibility zone extends to temperatures lower than the glass melting point - and gives a metastable immiscibility zone in a wide composition range where phase separation occurs normally in an amorphous state. In the EZDF, it may be expected

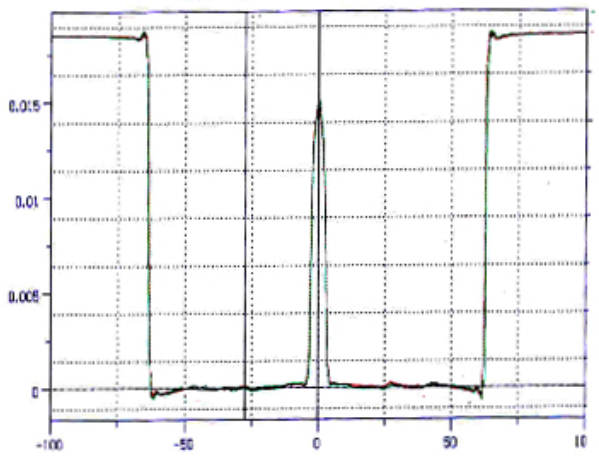

FIG. 1 Refractive index profile of fiber (ZEr-B).

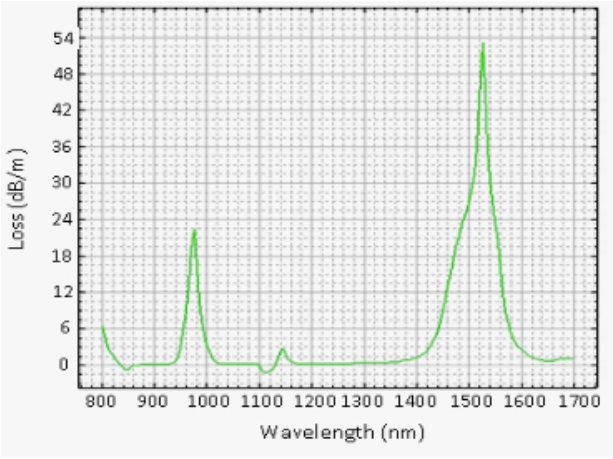

FIG. 2 Spectral attenuation curve of fiber (ZEr-B).

Perform No	Al_2O_3 (mole %)	ZrO_2 (mole %)	Er_2O_3 (mole %)
ZEr-A	0.25	0.65	0.155
ZER-B	0.24	2.10	0.225

TABLE 1 Doping levels within core region of the preforms

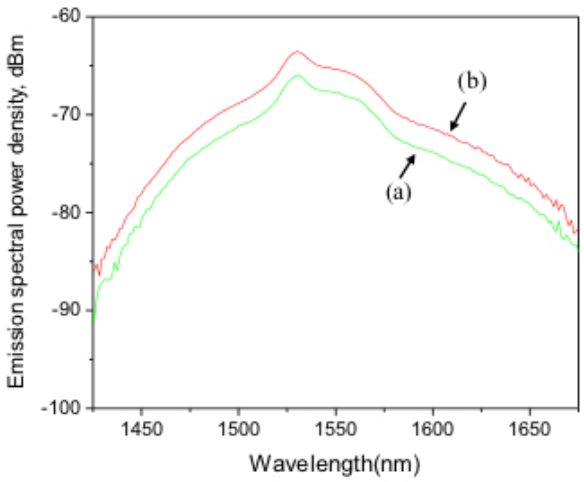

FIG. 3 Fluorescence curves of (a) fiber ZEr-A and (b) fiber ZEr-B at a pump power level of 100 mW.

that the separated ZrO_2 and Al_2O_3 phases would mix together into a homogeneous mixture before crystallization could occur during heating at high temperature, since the homogeneous amorphous mixture of compositions, $ZrAl_xO_y$, is generally thermodynamically more stable than the two separate phases. In this work two Er_2O_3 doped fibers, designated ZEr-A and ZEr-B, were fabricated. Both fibers contain 0.24-0.25 mole % of Al_2O_3, with the ZrO_2 and Er_2O_3 dopant concentration increased from 0.65 to 2.21 mole % and from 0.155 to 0.225 mole % for ZEr-A and ZEr-B respectively. The doping levels of the two fibers are obtained through an Electron Probe Micro-Analysis (EPMA) for both the fabricated fiber samples and is given in Table 1, whilst the physical parameters of the fibers are given in Table 2.

The measured refractive index profile of fiber ZEr-B is shown in Figure 1. The spectroscopic properties such as absorption coefficient, fluorescence and fluorescence decay curves of the fabricated fibers are measured, and it can be observed that the peak absorption of the two types of fiber at 978 nm are found to be 15.0 and 22.0 dB/m respectively. The spectral attenuation curve of fiber ZEr-B is shown in Figure 2, as the non-linear properties of this fiber will be analysed in the following section.

The fluorescence spectra of the fiber samples were measured with lateral pumping, for a pump power level of 100 mW at 980 nm. The fluorescence curves for both fibers are shown in Figure 3 and the fluorescence decay curves of both fibers are shown in Figure 4.

The two fibers (ZEr-A and ZEr-B) show almost the same fluorescence live-times of 10.93 and 10.86 ms respectively. Fiber ZEr-B, which has higher doping levels of Er_2O_3 and ZrO_2 shows slight shorter fluorescence life-time. These results indicate that the concentration-quenching phenomenon that is typical of Er^{3+} ions is strongly reduced through an increase in the doping levels of ZrO_2. In the generation of the FWM effect in the zirconia-erbium doped silica fiber, the ZEr-B is used instead of the ZEr-A due to the higher ZrO_2 concentration, which will provide a better non-linear interaction.

4 GENERATION OF THE FWM EFFECT IN THE EZDF

The generation of the FWM effect in nonlinear fibers can be explained by using the coupled differential equations for the propagating amplitudes, including the contributions to phase mismatch due to XPM and SPM [34]. A well-known formula used for FWM estimation was originally derived by Hill et. al. [35] and reformulated later to include the phase-mismatch dependent efficiency by Shibata et. al. [36]. In the FWM process in glass, two chosen wavelengths (λ_{pump} and λ_{signal}) will generate a converted wavelength $\lambda_{\text{converted\_signal}} = 2\lambda_{\text{pump}} - \lambda_{\text{signal}}$. To analyze the nonlinearity in the EZDF, the nonlinear coefficient, γ, is estimated by using;

$$\gamma = \sqrt{P_{textFMW}}\eta P_S P_P^2 e^{-\alpha L} L_{texteff^2} \quad (1)$$

Fiber Number	Core Composition	Core Diameter	Fiber Type	NA	A-eff	RI of core
ZEr-A	$SiO+Al_2O_3+P_2O_5$-ZrO_2-$Y_2O_3+Er_2O_3$	10.5	Circular core with normal resin	0.17	87 μ^2	1.46625
ZEr-B	$SiO+Al_2O_3+P_2O_5$-ZrO_2-$Y_2O_3+Er_2O_3$	10.0	Circular core with normal resin	0.20	75 μ^2	1.47025

TABLE 2 Fiber parameters

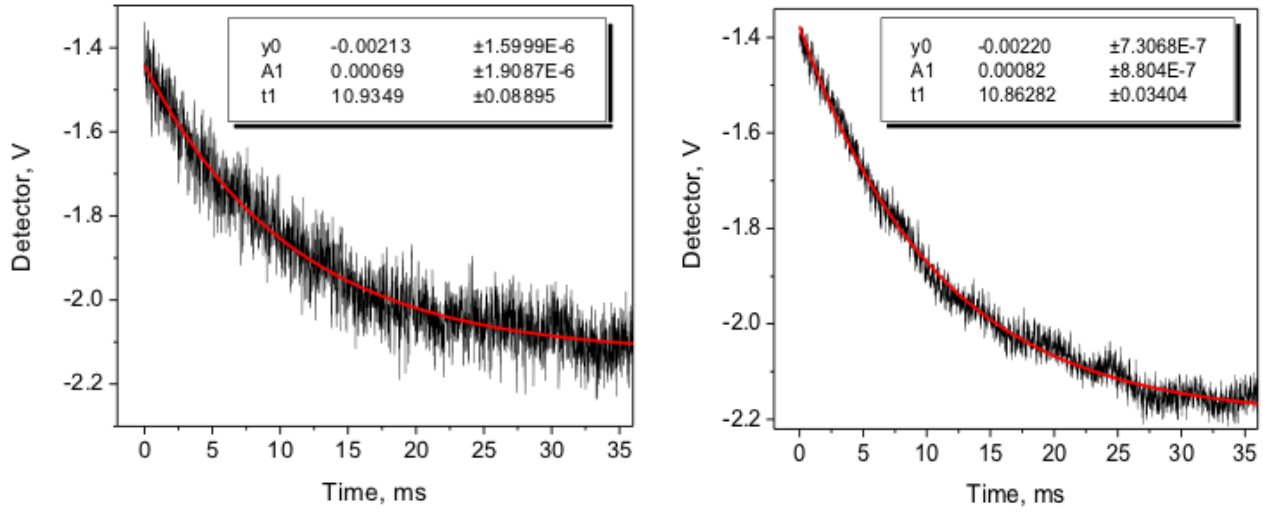

(a) (b)

FIG. 4 The fluorescence decay curve of two EDFs (a) ZEr-A and (b) ZEr-B at a pump power level of 100 mW.

where $P_{\mathrm{FWM}}|$ is the FWM power, P_P is the input pump power, P_S is the input signal power, L is the fiber length and α is the fiber attenuation coefficient. The effective length of the fiber L_{eff} takes into account the decrease in power due to attenuation - and is defined as;

$$L_{eff} = \frac{1 - e^{-\alpha L}}{\alpha} \tag{2}$$

The normalized FWM efficiency, η, is written as;

$$\eta = \frac{\alpha^2}{\alpha^2 + \Delta\beta^2}\left[1 + \frac{2e^{-\alpha L}\left(1 - \cos\left(\Delta\beta L\right)\right)}{\left(1 - e^{\alpha L}\right)^2}\right] \tag{3}$$

where is the phase $\Delta\beta$ mismatch that is given by;

$$\Delta\beta = \frac{2\pi\lambda^2}{c} D\Delta f^2 \tag{4}$$

with the dispersion parameter, $D = \frac{-2\pi c}{\lambda^2}\beta^2$, where β^2 is the group velocity dispersion parameter. From equation (4), it can be seen that P_{FMW} is at its minima when $\Delta\beta\frac{L}{2} = k\pi$, where k is an integer. This occurs due to the phase mismatch between the signals propagating inside the fiber and occurs at every $\frac{2\pi}{\beta}$ meters. The P_{FMW} minima can also be determined as a product of the channel spacing, such that:

$$\Delta f_k = \sqrt{\frac{kc}{\lambda^2 DL}} \tag{5}$$

As the magnitude of the nonlinearity in the fiber only shifts the P_{FMW} minima, therefore an analysis of the FWM signal power minima can be used to determine the dispersion of the optical fiber, whilst the nonlinearity can be estimated from the total fiber attenuation. The physical setup for measuring the P_{FMW} minima is simple and only requires two laser diodes with a tuning range of less than 1 nm each and a EZDF of the proper length. The channel spacing at which P_{FMW} reaches its first minima is a necessary measurement in calculating the dispersion of the fiber and is given as:

$$D = \frac{c}{\lambda^2 \Delta f^2 L} \tag{6}$$

From equations (1) to (6), the theoretical FWM power can now be calculated as

$$P_{\mathrm{FMW}} = \eta\gamma^2 P_p^2 P_s e^{-\alpha L} L_{eff}^2 \tag{7}$$

γ is determined by bi-directional measurements of the FWM power, while the chromatic dispersion is determined from the wavelength detuning of the FWM Power Conversion Efficiency (PCE). Both measurements use the same experimental setup as given by the schematic in Figure 5.

In the setup, two Yokogawa (AQ2200) Tunable Laser Sources (designated TLS1 and TLS2), with tuning ranges from 1460 nm to 1640 nm and linewidths of 0.015 nm are used as signal sources. The pump signal P_1 (or P_P), is generated by TLS 1 at a fixed wavelength of 1560 nm and an average output power of 12.8 dBm. A second signal, P_s is generated from TLS2 with a wavelength varying from 1561 nm to 1565 nm at an average power level of 10.8 dBm. Both P_1 and P_s are combined using a 3 dB coupler and a Polarization Controller (PC) to adjust the polarization of the input signals in order to obtain the maximum FWM efficiency. Additionally, two Laser Diode (LD) pumps at wavelengths of 1460 nm and 1490 nm are also launched into the EZDF using a WDM to excite the Er^{3+} ions just enough so that they are transparent to the

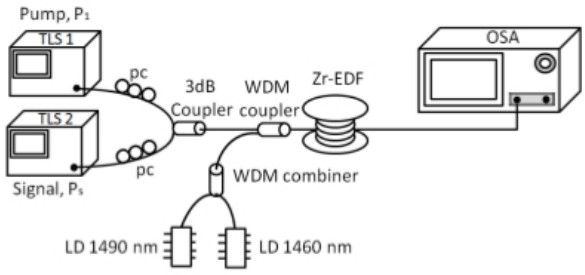

FIG. 5 Schematic diagram for generating FWM effects in the EZDF

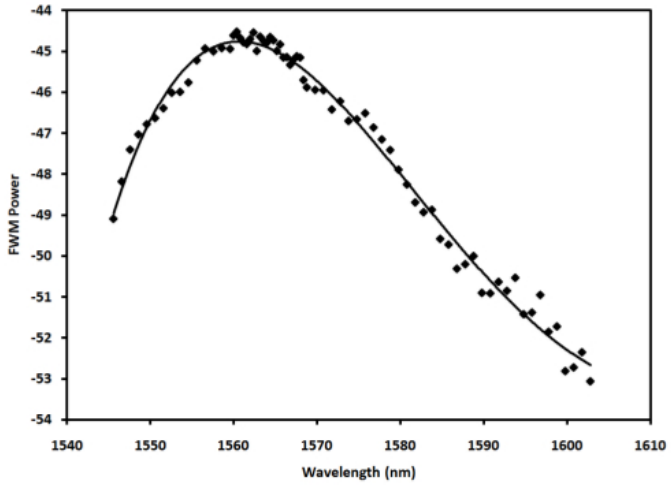

FIG. 6 The spectrum of the converted signal (FWM power) against the wavelength of the pump against converted wavelength for the ZEr-B optical fiber sample.

signals used for the generation of the FWM (the suppression of the Er^{3+} ions is necessary as the EZDF sample incorporates both ZrO_2 and Er_2O_3, however this work is only interested in the non-linear effects generated by the ZrO_2 in the fibre). A 4 m long ZEr-B fiber with an Erbium concentration of 3000 ppm is used. The ZEr-B fiber has a core refractive index value of 1.466 and an effective area of 87 μm^2 along with a propagation loss, α of 0.68 dB/m, which is obtained using the cut-back method. The refractive index and glass core size of the ZEr-B fiber used are important parameters that will be used to determine the nonlinearity of the fiber. Finally, a Yokogawa Optical Spectrum Analyzer (OSA) with 0.02 nm resolution bandwidth is used to measure the generated FWM spectrum.

5 RESULTS AND DISCUSSION

The power of signals generated by the FWM process is dependent the wavelength of the pump and input signal. In this work, the pump and signal wavelengths are detuned by 0.4 nm. The pump and signal powers are set at +15 dBm and +13 dBm respectively and are optimized for the maximum possible power using a PC. Figure 6 shows the power of the signal obtained from the FWM process against the pump wavelength.

It can be seen that the power of the converted signal begins to increase from a low value of -48 dBm at a pump wavelength of 1545 nm to a peak power of -45 dBm at 1565 nm. The power of the converted signal does not change signifcantly between 1558 nm to 1565 nm, with only minor fluctuations of approximately 0.5 dB being observed. After this region however, the power decreases rapidly as the pump power continues to increase towards the L-band region. The reason for this is that the gain spectrum of ZEr-B provides the highest gains at a wavelength around 1560 nm. As such, the pump signal is set at a wavelength of 1560 nm, as this will ensure the generation of the FWM output will fall within the flat region. The wavelength value of 1560 nm is also used in the measurement of the nonlinearity coefficient of ZEr-B.

Figure 7 shows the overlay spectrum of the converted signals along with the pump and signal wavelengths. The spectrum shown is as obtained from the OSA with a +25 dB fixed attenuator, the attenuator serving to protect the OSA from spikes in the signal which could potentially damage it. The pump wavelength is left constant at 1560 nm and -9.9 dBm power while the signal wavelengths are varied from 1561 nm to 1565 nm in steps of 1 nm. The power of the signal wavelength is maintained at -10.5 dBm. From Figure 7, it can be seen that two sidebands C_1 and S_2 are generated by the pump and signal wavelengths. At a signal wavelength of 1561 nm, two converted wavelengths are observed at 1559 nm (C_1) and 1562 nm (S_2), a shift of 2 and 1 nm respectively on either side of the signal. As the signal wavelength increases to 1562 nm, the converted wavelengths also shift accordingly to 1558 nm (C_1) and 1564 nm (S_2), giving a shift of 4 and 2 nm respectively. This trend is seen to continue as the signal wavelength continues to be varied until 1565 nm, which sees the C_1 move towards a wavelength of 1555 nm in steps of 1 nm, and S_2 increasing in steps of 2 nm to a wavelength of 1570 nm. It is also observed that when the signal wavelength increases at a fixed pump wavelength, the power of the generated sidebands drops. This can be attributed to the gain spectrum of the ZEr-B fiber such that the longer signal wavelengths move away from the optimum gain region of the fiber. The channel spacings obtained in Figure 8 are essential in determining the fiber non-linear coefficient, dispersion and slope dispersion of the ZEr-B fiber, which is seen in the following results.

Figure 8 shows the power of the converted signal, C_1 against the wavelength of the input signal. The pump is left constant at a wavelength of 1560 nm and the signal wavelength is varied from 1550 nm to 1559 nm with a frequency spacing 0.2 nm. To ensure the maximum power is obtained for the converted signal, the two PCs as shown in Figure 6 are adjusted to provide the optimum output power. As can be seen from the figure, the power of the converted signal is initially low at about -58 dBm. However, as the signal wavelength increases, so does the power of the converted signal, reaching a power of approximately -45 dBm at a wavelength of 1559 nm. Further increases in the input signal wavelength do not result in any change to the converted signal power. It can be seen that the experimental results agree well with the theoretical predictions for ZEr-B. It is observed that the difference in the power of the converted signal in Figure 9 and that of Figure 8 is attributed to the use of the +25 dB attenuator.

The analysis of FWM power in a function of channel spacing can be used to estimate the fiber chromatic dispersion

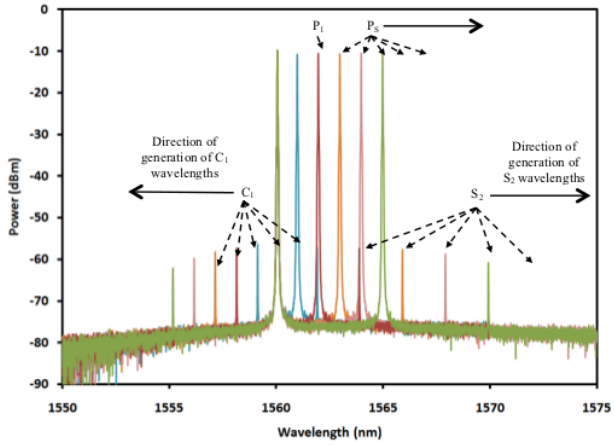

FIG. 7 The typical output spectra at P_1 and P_s, as well as their converted signals (sideband fields) C_1 and S_2 when wavelength of P_1 is fixed at 1560 nm and the wavelength of P_s is varied from 1561 nm to 1565 nm for the ZEr-B optical fiber sample.

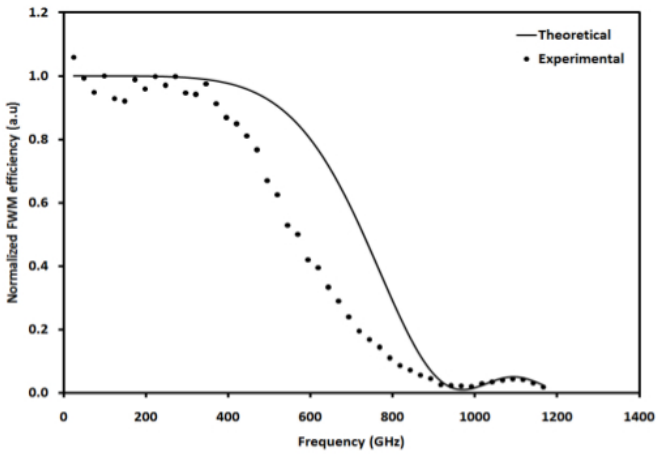

FIG. 9 Normalized FWM efficiency against the input signal frequency for the ZEr-B optical fiber sample.

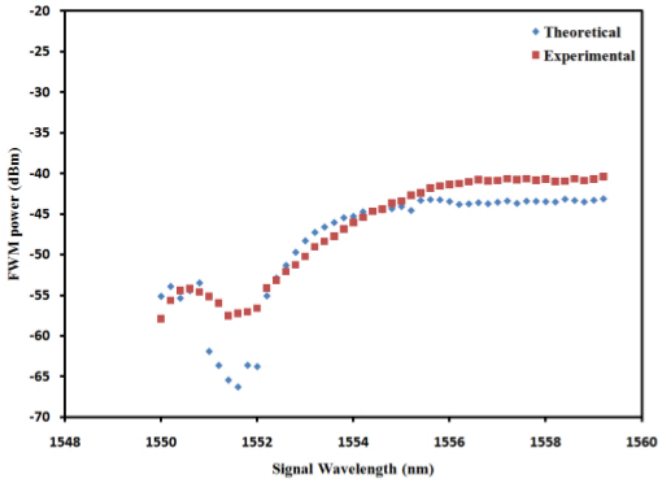

FIG. 8 FWM conversion efficiency versus wavelength detuning for the ZEr-B optical fiber sample.

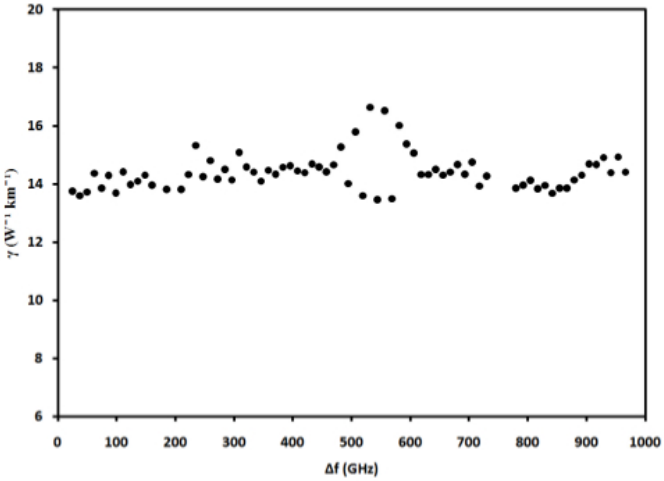

FIG. 10 Nonlinear coefficients with varying the frequency spacing as obtained using the ZEr-B optical fiber sample.

and dispersion slope. Figure 9 shows the normalized FWM efficiency against the input signal frequency. It can be seen that as the channel spacing (frequency) is increased from 30 GHz to 400 GHz, the FWM efficiency remains relatively the same, with fluctuations of about 0.5 a.u. However, above 400 GHz, the FWM efficiency begins to drop, reaching almost 0 at 1000 GHz. These measurements are in agreement with the theoretical predictions for the ZEr-B fiber. From equation (6) and the Figure 9, a chromatic dispersion and slope dispersion value of 28.45 ps/nm.km and 3.63 ps/nm^2.km respectively is obtained for ZEr-B.

Using the signal power, pump power, converted power and the normalized FWM efficiency, the nonlinear coefficient for Zr-EDF is estimated using equation (1). In this equation, the FWM efficiency is important in getting the value of nonlinear coefficient where it used equation (3) for found the value. Therefore, a nonlinear coefficient value of 14 W^{-1}km^{-1} is obtained for the ZEr-B. Figure 10 shows the variation of the nonlinear coefficient against the channel spacing.

From Figure 10, it can be seen that the non-linear coefficient remains the same for almost all channel spacing values, with the largest variation being approximately 2 dBm between the region of 500 to 600 GHz. This gives the ZEr-B fiber a high potential as a medium for a variety of applications such as wavelength conversion and wavelength generation.

6 CONCLUSIONS

The fabrication of an EDZF is described in the work, followed by an analysis of its application as a non-linear medium for the generation of the FWM effect. The fabrication of the EZDF follows the conventional approach with the creation of a standard silica preform using the MCVD technique. Glass modifiers and nucleating agents are then added to the silica preform using the solution doping technique and the resulting preform is annealed and drawn into a fiber strand with a diameter 125 $\pm$ 0.5 μm. In this work, two EZDF samples are fabricated and designated as ZEr-A and ZEr-B, with ZrO_2 and Er_2O_3 dopant concentrations of 0.65 to 2.21 mole % and 0.155 to 0.225 mole % respectively and numerical apertures of between 0.17 to 0.20 as well as peak absorptions of 15.0

and 22.0 dB/m respectively at 978 nm. In investigation FWM effect, a 4 m long portion of ZEr-B with a propagation loss of 0.68 dB/m and an erbium concentration of 3000 ppm is used. FWM power levels of approximately -45 dBm at around 1565 nm are obtained and agree well with the theoretical predicted values. The ZEr-B fiber also shows a non-linear coefficient of 14 $W^{-1}km^{-1}$ along with chromatic and dispersion slopes of 28.45 ps/nm.km and 3.63 ps/nm^2.km that are well in accordance to the theoretical values.

References

[1] G. E. Keiser, "A Review of WDM Technology and Applications," Opt. Fiber Technol. **5**, 3–39 (1999).

[2] M. Wasfi, "Optical Fiber Amplifiers – Review," Int. J. Comm. Netw. Infor. Sec. **1**, 42–47 (2009).

[3] H. Ahmad, M. Z. Zulkifli, A. A. Latif, K. Thambiratnam, and S. W. Harun, "17-channels S band multiwavelength Brillouin/Erbium Fiber Laser Co-Pump with Raman source," Laser Phys. **19**, 2188–2193 (2009).

[4] D. Richardson, J. Nilsson, and W. Clarkson, "High Power Fiber Lasers: Current Status and Future Perspectives [Invited]," J. Opt. Soc. Am. B **27**, 63–92 (2010).

[5] K. Inoue, and H. Toba, "Wavelength Conversion Experiment using Fiber Four-Wave Mixing," IEEE Photonic. Tech. L. **4**, 69–72 (1992).

[6] E. Yahel, and A. Hardy, "Amplified Spontaneous Emission in High-Power, Er^{3+}.Yb^{3+} Codoped Fiber Amplifiers for Wavelength-Division-Multiplexing Applications," J. Opt. Soc. Am. B **20**, 1198–1203 (2003).

[7] D. Cotter, and A. D. Ellis, "Asynchronous Digital Optical Regeneration and Networks," J. Lightwave Technol. **16**, 2068–2080 (1998).

[8] S. Abbott, "Review of 20 Years of Undersea Optical Fiber Transmission System Development and Deployment since TAT-8," in *Proceedings to Optical Communication, 2008. ECOC 2008. 34th European Conference on,* 1–4 (ECOC, Brussel, 2008).

[9] K. Rottwitt, and J. H. Povlsen, "Analysing the Fundamental Properties of Raman Amplifiers in Optical Fibers," J. Lightwave Technol. **23**, 3597–3613 (2005).

[10] J. H. Lee, Y. M. Chang, Y. G. Han, H. Chung, S. H. Kim, and S. B. Lee, "A Detailed Experimental Study on Single Pump Raman/EDFA Hybrid Amplifiers: Static, Dynamic, and System Performance Comparison," J. Lightwave Technol. **23**, 3848 (2005).

[11] P. Doussiere, A. Jourdan, G. Soulage, P. Garabedian, C. Graver, T. Fillion, E. Derouin, and D. Leclerc, "Clamped Gain Travelling Wave Semiconductor Optical Amplifier for Wavelength Division Multiplexing Applications," in *Proceedings to Semiconductor Laser Conference, 1994., 14th IEEE International,* 185–186 (IEEE, Maui, 1994).

[12] K. Morito, "Output-Level Control of Semiconductor Optical Amplifier by External Light Injection," J. Lightwave Technol. **23**, 4332–4341 (2005).

[13] T. Torounidis, P. A. Andrekson, and B.-E. Olsson, "Fiber-optical parametric amplifier with 70-dB gain," IEEE Photonic. Tech. L. **18**, 1194–1196 (2006).

[14] J. M. Chavez Boggio, P. Dainese, F. Karlsson, and H. L. Fragnito, "Broad-Band 88% Efficient Two-Pump Fiber Optical Parametric Amplifier," IEEE Photonic. Tech. L. **15**, 1528–1530 (2003).

[15] Y. Ohishi, A. Mori, M. Yamada, H. Ono, Y. Nishida, and K. Oikawa, "Gain Characteristics of Tellurite-Based Erbium-Doped Fiber Amplifiers for 1.5-μm Broadband Amplification," Opt. Lett. **23**, 274 (1998).

[16] S. Jiang, B.-C. Hwang, T. Luo, K. Seneschal, F. Smektala, S. Honkanen, J. Lucas, and N. Peyghambarian, "Net Gain of 15.5 dB from a 5.1 cm-Long Er^{3+} Doped Phosphate Glass Fiber," in *Proceedings to Optical Fiber Communications*, PD5–1 (IEEE, Baltimore, 2000).

[17] A. Cucinotta, F. Poli, and S. Selleri, "Design of Erbium-Doped Triangular Photonic-Crystal-Fiber-Based Amplifiers," IEEE Photonic. Tech. L. **16**, 2027 (2004).

[18] S. Aozasa, H. Masuda, and M. Shimizu, "S-band Thulium-Doped Fiber Amplifier Employing High Thulium Concentration Doping Technique," J. Lightwave Technol. **24**, 3842–3848 (2006).

[19] S. W. Harun, N. Tamchek, S. Shahi, and H. Ahmad, "L-band Amplification and Multi-Wavelength Lasing with Bismuth-Based Erbium Doped Fiber," Prog. Electromagn. Res. **6**, 1–12, (2009).

[20] S. D. Emami, P. Hajireza, F. Abd-Rahman, H. A. Abdul-Rashid, H. Ahmad, and S. W. Harun, "Wide-Band Hybrid Amplifier Operating in S-Band Region," Prog. Electromagn. Res. **102**, 301–313 (2010).

[21] E. Snoeks, P. G. Kik, and A. Polman, "Concentration Quenching in Erbium Implanted Alkali Silicate Glass," Opt. Mater. **5**, 159 (1996).

[22] D. M. Gill, L. McCaughan, and J. C. Wright, "Spectroscopic Site Determinations in Erbium-Doped Lithium Niobate," Phys. Rev. B **53**, 2334 (1996).

[23] M. C. Paul, S. W. Harun, N. A. D. Huri, A. Hamzah, S. Das, M. Pal, S. K. Bhadra, H. Ahmad, S. Yoo, M. P. Kalita, A. J. Boyland, and J. K. Sahu, "Wideband EDFA Based on Erbium Doped Crystalline Zirconia Yttria Alumino Silicate Fiber," J. Lightwave Technol. **28**, 2919–2924 (2011).

[24] M. C. Paul, S. W. Harun, N. A. D. Huri, A. Hamzah, S. Das, M. Pal, S. K. Bhadra, H. Ahmad, S. Yoo, M. P. Kalita, A. J. Boyland, and J. K. Sahu, "Performance comparison of Zr-based and Bi-based erbium-doped fiber amplifiers," Opt. Lett. **35**, 2882–2884 (2010).

[25] J. R. Armitage, "Spectral Dependence of the Small-Signal Gain around 1.5 μm in Erbium Doped Silica Fiber Amplifiers," IEEE J. Quantum Electron. **26**, 423–425 (1990).

[26] B. Pedersen, A. Bjarklev, J. H. Povlsen, K. Dybdal, and C. C. Larsen, "The design of erbium-doped fiber amplifiers," J. Lightwave Technol. **9**, 1105–1112 (1991).

[27] J. Yang, S. Dai, Y. Zhou, L. Wen, L. Hu, and Z. Jiang, "Spectroscopic Properties and Thermal Stability of Erbium-Doped Bismuth-Based Glass for Optical Amplifier," J. Appl. Phys. **93**, 977–983 (2003).

[28] P. Peterka, B. Faure, W. Blanc, M. Karásek, and B. Dussardier, "Theoretical Modelling of S-band Thulium-Doped Silica Fibre Amplifiers," Opt. Quant. Electron **36**, 201–212 (2004).

[29] K. Kikuchi, and C. Lorattanasane, "Design of Highly Efficient Four-Wave Mixing Devices using Optical Fibers," IEEE Photonic. Tech. L. **6**, 992–994 (1994).

[30] O. Aso, A. Shin-Ichi, T. Yagi, M. Tadakuma, Y. Suzuki, and S. Namiki, "Broadband Four-Wave Mixing Generation in Short Optical Fibres," Electron. Lett. **36**, 709–711 (2000).

[31] G. D. Wilk, R. M. Wallace, and J. M. Anthony, "Hafnium and Zirconium Silicates for Advanced Gate Dielectrics," J. Appl. Phys. **87**, 484–492 (2000).

[32] G. Rayner, R. Therrien, and G. Lucovsky, "The structure of plasma-deposited and annealed pseudo-binary ZrO_2-SiO_2 alloys," Proc. Mater. Res. Soc. Symp. **611**, C1.3.1–C1.3.9 (2000).

[33] P. F. James, "Liquid-Phase Separation in Glass-Forming Systems," J. Mater. Sci. **10**, 1802–1825 (1975).

[34] G. P. Agrawal, *Nonlinear Fiber Optics* (Academic Press, London, 1995).

[35] K. O. Hill, D. C. Johnson, B. S. Kawasaki, and R. I. MacDonald, "CW Three-Wave Mixing in Single-Mode Fibers," J. Appl. Phys. **49**, 50980–51006 (1978).

[36] N. Shibata, R. P. Braun, and R. G. Warrts, "Phase-Mismatch Dependence of Efficiency of Wave Generation through Four-Wave Mixing in a Singlemode Fiber," Quantum Electron. **23**, 1205–1211 (1987).